Supporting Information Appendix

Structural determinants in phycotoxins and AChBP conferring high affinity binding and nicotinic AChR antagonism

Yves Bourne, Zoran Radic', Rómulo Aráoz, Todd T. Talley, Evelyne Benoit, Denis Servent, Palmer Taylor, Jordi Molgó, & Pascale Marchot

Supplemental Results

Characteristics of SPX and GYM binding to nAChRs. The 150 μM EC_{50} value determined for ACh effect on the neuronal α4β2 suggests assembly of a majority of the low sensitivity $\alpha4_3\beta2_2$ subpopulation (relative to the high sensitivity $\alpha4_2\beta2_3$ subpopulation) upon transfection (38, 39). In turn, the 25 μM value and usual desensitization event found for the muscle-type $\alpha1_2\beta\gamma\delta$ attest for full functionality of both the high and low affinity ACh binding sites on the transplanted nAChR.

The Hill coefficient of ~2 found for inhibition of α4β2 currents by SPX and GYM may be indicative of toxin binding at each of the two α-β interfaces. Should an additional α-α interface be present in the transfected receptors (cf above), it may also be involved in toxin binding since eight of the ten residues important for toxin binding to A-AChBP are conserved in the α4 and β2 sequences (cf. Results, and Fig. S1). In contrast, the Hill coefficient of ~1 and the unaltered desensitization component found for inhibition of the $\alpha1_2\beta\gamma\delta$ currents suggest toxin binding to one subunit interface only. This could be the αδ interface since two of the ten residues important for toxin binding to A-AChBP (Lys143 and Tyr195) are conserved in the δ subunit, but not the γ subunit (cf. Results, and Fig. S1).

As a control assay with a reference organic antagonist we explored d-tubocurarine inhibition of ACh-evoked currents in the $\alpha1_2\beta\gamma\delta$-transplanted oocytes. The dose-response curve (Fig. S2), with its Hill coefficient of ~1, is again indicative of antagonist binding to one interface only. Both this value and the IC_{50} value are consistent with those issued from electrophysiological recordings of d-tubocurarine-induced ACh-blockade of expressed (from transfected cDNAs) Torpedo nAChR (cf. Fig. 4D in (40)). Moreover, the IC_{50} value, greater by 72- and 13-fold than those for inhibition of the $\alpha1_2\beta\gamma\delta$ currents by SPX and GYM, respectively (cf. Table 2), reflects less potent antagonism by d-tubocurarine than by the SPX and GYM toxins for this nAChR subtype. Therefore it appears that data obtained with Torpedo nAChR either micro-transplanted or expressed in oocytes are comparable if not similar. This largely confirms that the micro-transplantation approach is valid and has several advantages with respect to heterologously expressed receptors, as recently pointed out (41).

Supplemental Discussion

Spirolide congeners. The structure of the SPX-AChBP complex, in revealing a requirement for a cyclic imine for efficient AChBP and nAChR binding, illustrates why spirolides E and F, that are keto-amine hydrolysis products of ring opening of the cyclic imine unit, are non toxic (5). Furthermore, the complete loss of toxicity observed upon reducing GYM to produce gymnodamine (=N- converting to -NH-) suggests that the cyclic imine functionality is the key determinant of GYM (42) to primarily H bond with the carbonyl oxygen of the conserved Trp 147 as observed for SPX.

Other members of the spirolide family, such as spirolide G (8) and 20-methylspirolide G (6)

which contain a 5,6,6-*bis*-spiroacetal ring system as opposed to the 5,5,6 system found in SPX and other spirolides, and pinnatoxins (PnTx) or pteriatoxins (PtTx), would be expected to bind in a similar way as SPX. However, an unfavorable position of the methylene at the C17 position coupled to the additional allylic hydroxyl at C18 in the gymnodimine-B macrocycle (Fig. 1) may result in steric clashes with the interacting residues from loop E, consistent with a 10-fold lower toxicity in mice compared to GYM (15). Similarly, the additional hydroxyl group within the solvent-buried branch of the 27-hydroxy-13,19-didesmethyl spirolide C congener (1) may lead to steric clashes with the larger side chains of Tyr147 from the (+) face and Tyr55 and Ile118 from the (-) face. Spirolide H contains a dispiroketal ring system in place of the trispiroketal ring system of spirolides A-G. Beside presence of an additional methyl group on the proximal tetrahydrofuran ring, the molecular bases of the loss of toxicity of this congener in the mouse assay remain to be investigated (43).

Supplemental Materials and Methods

Live animals and biological materials. *Torpedo marmorata* and adult female *Xenopus laevis* frogs were purchased live from the Station Biologique de Roscoff (France) and the Centre de Ressources Biologiques Xénopes (Rennes, France), respectively. Animals were maintained and treated according to the European standard protocols approved by the Animal Ethics Committee of the CNRS. Experiments were performed in accordance with European Community guidelines for laboratory animal handling and with the official edict presented by the French Ministry of Agriculture and the recommendations of the Helsinski Declaration.

The cDNAs encoding the human α3β2 and α4β2 nAChRs were kindly provided by Prof. J. P. Changeux (Pasteur Institute, Paris) and Prof. O. Steinlein (Institute of Human Genetics, Bonn), respectively. The SPX and GYM toxins were obtained from the National Research Council Canada. They were found ~ 95% homogeneous by ^{1}H-NMR and LC-MS. Stock solutions in acidified methanol were titrated by quantitative NMR. ^{125}I-BgTx and [^{3}H]-EPI were from PerkinElmer and [^{3}H]-MLA from American Radiolabeled Chemicals Inc.

nAChR binding assays. IC_{50} values were determined by fitting the competition data to a binding isotherm and conversion to Ki constants using equation: $Ki = IC_{50}/(1+L^*/K_d)$ (equ. 1) (44), and K_d values of 50 pM for ^{125}I-BgTx binding on $\alpha1_2\beta\gamma\delta$ and of 35 pM and 20 pM for [^{3}H]-EPI binding on α3β2 and α4β2, respectively.

Voltage-clamp recording on oocytes. Nicotinic currents were recorded with a two-microelectrode voltage-clamp amplifier (OC-725B, Warner Instrument Corp., Hamden, CT). Voltage and current microelectrodes were pulled from borosilicate glass to reach 0.5-1.5 MΩ tip resistance when filled with 3 M KCl. Data were acquired with a pCLAMP-9/Digidata-1322A system (Molecular Devices, Union City, CA). The recording chamber (capacity 300 µl) was superfused (8-12 ml/min; 20°C) with a modified Ringer's solution (5 mM HEPES, pH 7.4, 100 mM NaCl, 2.8 mM KCl, 0.3 mM $BaCl_2$) where $BaCl_2$ substitution to $CaCl_2$ prevents secondary activation of a Ca^{2+}-dependent Cl^- current (45). Oocytes were initially incubated for 2 min with SPX or GYM, and then freshly diluted ACh was applied for 5 or 7 s using a computer-controlled solution-exchange system (VC-6, Warner Instruments). Between successive ACh applications, 2.5 min perfusion intervals with modified Ringer's were maintained to insure receptor recovery from desensitization.

Concentration-inhibition analysis of ACh currents. Dose-response curves for agonist activation were analysed using equation: $I = I_{max}[L]^n/(EC_{50} + [L])^{nH}$ (equ. 2), where I is the measured agonist-evoked current, [L] is the agonist concentration, EC_{50} is the agonist concentration that evoked half the maximal current (I_{max}) and nH is the Hill coefficient. I values were normalized to the I_{max} value recorded from the same oocyte, to yield fractional (%) response data. The IC_{50} was determined from

dose-response curves by fitting to equation: $F = 1/[1+([X]/IC_{50})^{nH}]$ (equ. 3), where F is the fractional response obtained in presence of the inhibitor at concentration [X] and IC_{50} is the inhibitor concentration that reduced the ACh-evoked amplitude by half. Statistical significance of differences between controls and test values was assessed using the two-tailed Student's t-test or the Kolmogorov-Smirnov two-sample test and $p < 0.05$.

Expression of A- and L-AChBP and purification. Each AChBP, flanked with an N-terminal FLAG epitope numbered (-8)DYKDDDDKL(0), was expressed as a soluble exported protein using a synthetic cDNA and stably-transfected HEK293S-GnTI$^-$ cells selected for G418 resistance (24). Dulbecco's modified Eagle's medium (MediaTech CellGro) containing 2% FBS and the secreted AChBP was collected every 1-3 days for up to 4 weeks, supplemented with 0.02% NaN_3 and stored at 4°C. AChBP was purified on immobilized anti-FLAG M2 antibody (Sigma) (22) with elution using 100 μg/ml FLAG peptide in 50 mM Tris-HCl pH 7.4, 150 mM NaCl, 0.02% NaN_3. Purified AChBP was dialyzed against the same buffer and concentrated by ultrafiltration.

Ligand binding to AChBP. Measurement of k_{on}'s entailed direct admixture of reactants and monitoring the quenching of the protein native Trp fluorescence. Measurement of k_{off}'s used scavenging of free AChBP binding sites by an excess of competing ligand to form a non-quenching complex (22, 24). In brief, the equilibrated phycotoxin-AChBP complex at 250 pM in binding sites and slight molar excess of toxin was mixed with [^{3}H]-MLA (A-AChBP) or [^{3}H]-EPI (L-AChBP) at concentrations well above their respective K_d value to titrate those binding sites made available upon toxin dissociation. The time course of [^{3}H]-ligand binding was monitored over several hours. First order dissociation rate constants were determined by nonlinear regression of data using simple mono-exponential relationship. K_d's were calculated from the ratio of rate constants.

Crystallization and data collection. The complexes were formed with 240 μM AChBP in binding sites (~6 mg/ml) and a 1.25-fold molar excess of ligand (incubation: 1 h at 20-25°C, then overnight at 4°C). Crystallization was achieved by vapor diffusion at 18°C using 1 μl hanging drops and a 1:1 (v/v) protein-to-well solution ratio, with 27-30% PEG-400, 0.1 M HEPES, pH 7.5-7.7, 0.2 M $MgCl_2$ as the well solution. Crystals were directly flash-cooled in the nitrogen gas stream. Data were processed with HKL2000 (46) or XDS (47) and scaled/merged with XSCALE (47) or SCALA (48).

Structure determination and refinement. For each complex, the initial model obtained by molecular replacement was improved by manual adjustment with COOT (49) and refined with REFMAC (50) and TLS refinement with each subunit defining a TLS group. Random sets of reflections were set aside for cross-validation purposes. The molecular structures of SPX and GYM and the associated library files containing topological and parametric data were generated with SKETCHER (48). Automated solvent building was performed with COOT. The stereochemistry of each structure was analyzed with COOT and MOLPROBITY (51). Data collection and refinement statistics are reported in Table S2.

Structural comparisons. Comparison of the SPX- and GYM-A-AChBP complexes with other structures include those of A-AChBP in the apo form and in complex with the agonist EPI and antagonists MLA and α-conotoxin ImI (PDB codes, 2BYN, 2BYQ, 2BYR, 2BYP) (24) and that of the nicotine-L-AChBP complex (1UW6) (21). The average root mean square deviation between SPX- and GYM-bound AChBP subunits is 0.5 Å for 208 Cα atoms with largest deviation up to 2.4 Å for residue Cys191 located at the tip of loop C; between SPX-bound and the above-mentioned structures it is in the 0.6 - 1.3 Å range with largest deviation up to 9 Å for residue Cys190, vicinal to Cys191.

Supplemental references

38. Zwart R, Vijverberg HP (1998) Four pharmacologically distinct subtypes of α4β2 nicotinic acetylcholine receptor expressed in *Xenopus laevis* oocytes. *Mol Pharmacol* 54:1124-1131.
39. Moroni M, Zwart R, Sher E, Cassels BK, Bermudez I (2006) α4β2 nicotinic receptors with high and low acetylcholine sensitivity: pharmacology, stoichiometry, and sensitivity to long-term exposure to nicotine. *Mol Pharmacol* 70:755-768.
40. Xie Y, Cohen JB (2001) Contributions of *Torpedo* nicotinic acetylcholine receptor γTrp-55 and δTrp-57 to agonist and competitive antagonist function. *J Biol Chem* 276:2417-2426.
41. Eusebi F, Palma E, Amici M, Miledi R (2009) Microtransplantation of ligand-gated receptor-channels from fresh or frozen nervous tissue into *Xenopus* oocytes: A potent tool for expanding functional information. *Progr Neurobiol* 88:32-40.
42. Stewart M, Blunt JW, Munro MHG, Robinson WT, Hannah DJ (1997) The absolute stereochemistry of the New Zealand shellfish toxin gymnodimine. *Tetrahedron Lett* 38:4889-4890.
43. Roach JS, Leblanc P, Lewis NI, Munday R, Quilliam MA, Mackinnon SL (2009) Characterization of a dispiroketal spirolide subclass from *Alexandrium ostenfeldii*. *J Nat Prod* 72:1237-1240.
44. Cheng Y, Prusoff WH (1973) Relationship between the inhibition constant (K1) and the concentration of inhibitor which causes 50 per cent inhibition (I50) of an enzymatic reaction. *Biochem Pharmacol* 22:3099-3108.
45. Sands SB, Costa AC, Patrick JW (1993) Barium permeability of neuronal nicotinic receptor α7 expressed in *Xenopus* oocytes. *Biophys J* 65:2614-2621.
46. Otwinowski Z, Minor W (1997) Processing of X-ray diffraction data collected in oscillation mode. *Methods Enzymol* 276:307-326.
47. Kabsch W (1993) Automatic processing of rotation diffraction data from crystals of initially unknown symmetry and cell constants. *J Appl Cryst* 26:795-800.
48. CCP4 (1994) The CCP4 suite: Programs for protein crystallography. *Acta Crystallogr D Biol Crystallogr* 50:760-763.
49. Emsley P, Cowtan K (2004) Coot: model-building tools for molecular graphics. *Acta Crystallogr D Biol Crystallogr* 60:2126-2132.
50. Murshudov GN, Vagin AA, Dodson EJ (1997) Refinement of macromolecular structures by the maximum-likelihood method. *Acta Crystallogr D Biol Crystallogr* 53:240-255.
51. Davis IW, et al. (2007) MolProbity: all-atom contacts and structure validation for proteins and nucleic acids. *Nucleic Acids Res* 35:W375-W383.

Supplemental legend to Fig. 1

Legend to Fig. 1. Spirolide A, R_1 = H, R_2 = CH_3, R_3 = CH_3 ($\Delta^{2,3}$); spirolide B, R_1 = H, R_2 = CH_3, R_3 = CH_3; spirolide C, R_1 = CH_3, R_2 = CH_3, R_3 = CH_3 ($\Delta^{2,3}$); spirolide D, R_1 = CH_3, R_2 = CH_3, R_3 = CH_3 (4, 5). 13,19-didesmethyl spirolide C, R_1 = CH_3, R_2 = H, R_3 = H ($\Delta^{2,3}$); ($\Delta^{2,3}$) denotes presence of a single bond between C2 and C3 in the butyrolactone instead of the displayed double bond. Gymnodimine B, R_1 = CH_2, R_2 = OH, R_3 = H; gymnodimine C, R_1 = CH_2, R_2 = H; R3 = OH (12-15).

Supplemental figures

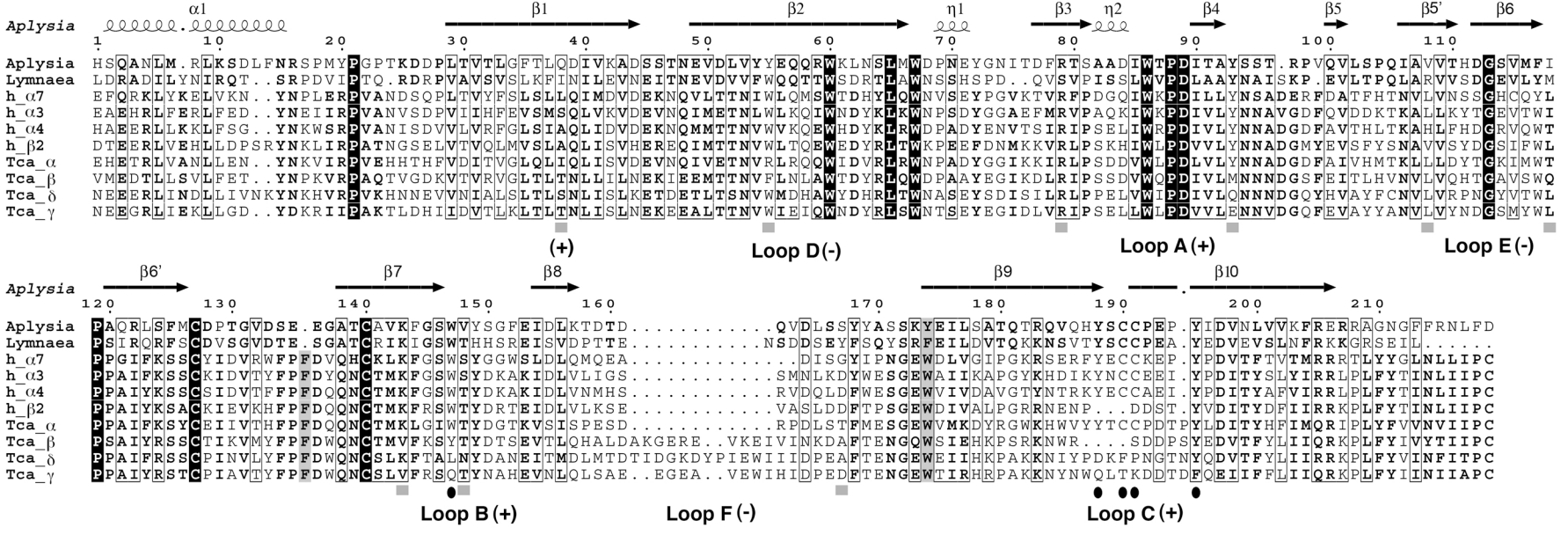
α1
β1
β2
η1
β3
η2
β4
β5
β5'
β6
Aplysia
1 10 20 30 40 50 60 70 80 90 100 110
Aplysia HSQANLM.RLKSDLFNRSPMYPGPTKDDPLTVTLGFTLQDIVKADSSTNEVDLVYYEQQRWKLNSLMWDPNEYGNITDFRTSAADIWTPDITAYSST.RPVQVLSPQIAVVTHDGSVMFI
Lymnaea LDRADILYNIRQT..SRPDVIPTQ.RDRPVAVSVSLKFINILEVNEITNEVDVVFWQQTTWSDRTLAWNSSHSPD..QVSVPISSLWVPDLAAYNAISKP.EVLTPQLARVVSDGEVLYM
h_α7 EFQRKLYKELVKN..YNPLERPVANDSQPLTVYFSLSLLLQIMDVDEKNQVLTTNIWLQMSWTDHYLQWNVSEYPGVKTVRFPDGQIWKPDILLYNSADERFDATFHTNVLVNSSGHCQYL
h_α3 EAEHRLFERLFED..YNEIIRPVANVSDPVIIHFEVSMSQLVKVDEVNQIMETNLWLKQIWNDYKLKWNPSDYGGAEFMRVPAQKIWKPDIVLYNNAVGDFQVDDKTKALLKYTGEVTWI
h_α4 HAEERLLKKLFSG..YNKWSRPVANISDVVLVRFGSLSIAQLIDVDEKNQMMTTNVWVKQEWHDYKLRWDPADYENVTSIRIPSELIWRPDIVLYNNADGDFAVTHLTKAHLFHDGRVQWT
h_β2 DTEERLVEHLLDPSRYNKLIRPATNGSELVTVQLMVSLAQLISVHEREQIMTTNVWLTQEWEDYRLTWKPEEFDNMKKVRLPSKHIWLPDVVLYNNADGMYEVSFYSNAVVSYDGSIFWL
Tca_α EHETRLVANLLEN..YNKVIRPVEHHTHFVDITVGLQLIQLISVDEVNQIVETNVRLRQQWIDVRLRWNPADYGGIKKIRLPSDDVWLPDLVLYNNADGDFAIVHMTKLLLDYTGKIMWT
Tca_β VMEDTLLSVLFET..YNPKVRPAQTVGDKVTVRVGLTLTNLLILNEKIEEMTTNVFLNLAWTDYRLQWDPAAYEGIKDLRIPSSDVWQPDIVLMNNNDGSFEITLHVNVLVQHTGAVSWQ
Tca_δ NEEERLINDLLIVNKYNKHVRPVKHNNEVVNIALSLTLSNLISLKETDETLTSNVWMDHAWYDHRLTWNASEYSDISILRLPPELVWTPDIVLQNNNDGQYHVAYFCNVLVRPNGYVTWL
Tca_γ NEEGRLIEKLLGD..YDKRIIPAKTLDHIIDVTLKLTLTNLISLNEKEEALTTNVWIEIQWNDYRLSWNTSEYEGIDLVRIPSELLWLPDVVLENNVDGQFEVAYYANVLVYNDGSMYWL
(+)
Loop D(-)
Loop A(+)
Loop E(-)
β6'
β7
β8
β9
β10
Aplysia
120 130 140 150 160 170 180 190 200 210
Aplysia PAQRLSFMCDPTGVDSE.EGATCAVKFGSWVYSGFEIDLKTDTD.....QVDLSSYYASSKYEILSATQTRQVQHYSCCPEP.YIDVNLVVKFRERRAGNGFFRNLFD
Lymnaea PSIRQRFSCDVSGVDTE.SGATCRIKIGSWTHHSRESISVDPTTE.....NSDDSEYFSQYSRFEILDVTQKKNSVTYSCCPEA.YEDVEVSLNFRKKGRSEIL.....
h_α7 PPGIFKSSCYIDVRWFPFDVQHCKLKFGSWSYGGWSLDLQMQEA.....DISGYIPNGEWDLVGIPGKRSERFYECCKEP.YPDVTFTVTMRRRTLYYGLNLLIPC
h_α3 PPAIFKSSCKIDVTYFPFDYQNCTMKFGSWSYDKAKIDLVLIGS.....SMNLKDYWESGEWAIIKAPGYKHDIKYNCCEEI.YPDITYSLYIRRLPLFYTINLIIPC
h_α4 PPAIYKSSCSIDVTFFPFDQQNCTMKFGSWTYDKAKIDLVNMHS.....RVDQLDFWESGEWVIVDAVGTYNTRKYECCAEI.YPDITYAFVIRRLPLFYTINLIIPC
h_β2 PPAIYKSACKIEVKHFPFDQQNCTMKFRSWTYDRTEIDLVLKSE.....VASLDDFTPSGEWDIVALPGRRNENP...DDST.YVDITYDFIIRRKPLFYTINLIIPC
Tca_α PPAIFKSYCEIIVTHFPFDQQNCTMKLGIWTYDGTKVSISPESD.....RPDLSTFMESGEWVMKDYRGWKHWVYYTCCPDTPYLDITYHFIMQRIPLYFVVNVIIPC
Tca_β PSAIYRSSCTIKVMYFPFDWQNCTMVFKSYTYDTSEVTLQHALDAKGERE..VKEIVINKDAFTENGQWSIEHKPSRKNWR....SDDPSYEDVTFYLIIQRKPLFYIVYTIIPC
Tca_δ PPAIFRSSCPINVLYFPFDWQNCSLKFTALNYDANEITMDLMTDTIDGKDYPIEWIIIDPEAFTENGEWEIIHKPAKKNIYPDKFPNGTNYQDVTFYLIIRRKPLFYVINFITPC
Tca_γ PPAIYRSTCPIAVTYFPFDWQNCSLVFRSQTYNAHEVNLQLSAE..EGEA..VEWIHIDPEDFTENGEWTIRHRPAKKNYNWQLTKDDTDFQEIIFFLIIQRKPLFYIINIIAPC
Loop B(+)
Loop F(-)
Loop C(+)

Supp. Fig1

Fig. S1 (above). Sequence alignment for the AChBPs and nAChRs related to this study. The secondary structure elements are labeled above the alignment. Loops A (or β4-β5), B (β7-β8), C (β9-β10), D (β2), E (β6-β6'), F (β8-β9) and the Cys-loop (β6'-β7) are indicated below the alignment. The location of the loops at the (+) or (-) faces of the subunit interface is indicated. A-AChBP residues whose side chains interact with the bound SPX and GYM molecules are indicated by a *filled circle* for those that are conserved in the nAChRs and a *grey square* for those that are not conserved.

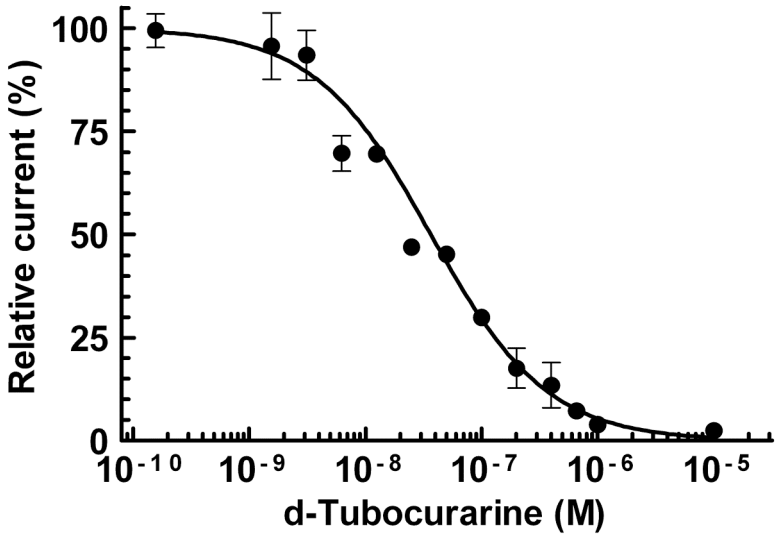

Fig. S2 (above). Inhibition, by d-tubocurarine, of ACh-evoked currents from the *Torpedo* $\alpha 1_2\beta\gamma\delta$ nAChR incorporated into the oocyte membrane. The amplitudes of the ACh-evoked current peaks recorded in the presence of d-tubocurarine (mean ± SEM; 3-5 oocytes per concentration) were normalized to control currents (25 μM ACh, 15 s perfusion) and fitted to the Hill equation (d-tubocurarine IC_{50} = 36.7 ± 0.9 nM; nH = 0.87 ± 0.12).

Supplemental tables

Table S1. Ratios of kinetic and equilibrium dissociation constants for SPX and GYM with A- and L-AChBP (calculated from the values reported in Table 3).

	A-AChBP	L-AChBP	SPX	GYM
Ratio of	SPX / GYM	SPX / GYM	L / A	L / A
k_{off}	1.1	222	20	0.1
k_{on}	0.27	0.25	0.31	0.35
K_d	4	923	63	0.28

Table S2. Data collection and refinement statistics for the SPX- and GYM- A-AChBP complexes.

	SPX	GYM
Data collection		
ESRF beamline	ID23-EH2	ID23-EH1
Wavelength (Å)	0.872	0.979
Space group	$P2_1$	$P2_12_12_1$
Cell dimensions a, b, c (Å) . β (°)	77.6, 131.7, 125.6 90.4	74.4, 124.3, 130.5 -
Resolution range(Å) [a]	20 - 2.5 (2.6 - 2.5)	15 - 2.4 (2.5 - 2.4)
Total observations	254 786	250 068
Unique reflections	85 373	47 713
Multiplicity	3.0 (2.7)	5.2 (5.2)
Completeness (%)	98.8 (94.0)	99.2 (96.6)
R_{sym}(%) [b]	9.1 (41.0)	9.9 (47.3)
$\langle I/\sigma(I)\rangle$	8.3 (1.9)	14.4 (3.9)
Refinement		
Resolution (Å)	20 - 2.5	15 - 2.4
No. reflections	83 509	45 448
R_{work}/R_{free} (%) [c]	17.6 / 23.6	17.9 / 23.3
No. atoms (protein/ligand/water)	17042 / 500 / 908	8628 / 185/ 392
Average B-factors (Å^2)		
Protein (main - side) / Ligand / Water	46.2 - 47.2 / 40.1 / 29.7	40.5 - 41.5 / 34.9 / 31.3
R.m.s.d. [d]		
Bond (Å)	0.009	0.008
Angles (°)	1.31	1.23
Chiral volume (A^3)	0.077	0.076
Ramachandran plot (%)		
Most favored regions	98.3	97.4
Additionally allowed regions	1.4	2.0
PDB code	2WZY	2X00

[a] Values in parentheses are those for the last shell.
[b] R_{merge} $\Sigma_{hkl}\Sigma_i \left| I_{i(hkl)} - \langle I_{hkl}\rangle \right| / \Sigma_{hkl}\Sigma_i I_{i(hkl)}$, where I is an individual reflection measurement and $\langle I\rangle$ is the mean intensity for symmetry-related reflections.
[c] $R_{cryst} = \Sigma_{hkl} \left| \left| Fo \right| - \left| Fc \right| \right| / \Sigma_{hkl} \left| Fo \right|$, where Fo and Fc are observed and calculated structure factors, respectively. R_{free} is calculated for 5% of randomly selected reflections excluded from refinement.
[d] Root-mean-square deviation from ideal values.

Table S3. Intermolecular interactions within a 4 Å distance between atoms in the bound SPX and GYM and in A-AChBP.

SPX	AChBP subunit interface	
	Principal (+) side	Complementary (-) side
bis-spiroacetal core	**Cys190**, **Cys191**, **Tyr195**, Val148	**Arg79**, Val108
solvent-buried branch	**Trp147**, Val148	Ile118
7-membered imine ring	**Trp147**, **Tyr93**, **Tyr188**, **Tyr195**	---
cyclohexene ring	**Tyr93**, **Trp147**	Tyr55
solvent-exposed branch	---	---
butyrolactone ring	**Lys143**, **Tyr93**, **Tyr188**	Gln38, Tyr55, Ser167

GYM	AChBP subunit interface	
	Principal (+) side	Complementary (-) side
tetrahydrofuran ring	**Tyr195**,	Val108, Ile118
solvent-buried branch	**Trp147**, Val148	Ile118
6-membered imine ring	**Trp147**, **Tyr93**, **Tyr188**, **Tyr195**	---
cyclohexene ring	**Tyr93**, **Trp147**	Tyr55
solvent-exposed branch	**Tyr188**, **Cys190**	---
butyrolactone ring	**Lys143**, **Tyr93**, **Tyr188**	Gln38, Tyr55, Ser167

In bold are A-AChBP residues that are invariant in the neuronal α3, α4 and α7 subunits. Residues Gln38, Tyr55, Arg79, Tyr93, Lys143, Val148, Ser167 and Cys190, but not Val108 and Ile118, are conserved between the α4 and β2 subunits.